

New Synthesis Method of a Si Nanocomposite Anode for Li-Ion Batteries

Laurence Lacroix-Orio, Monique Tillard,*
David Zitoun, and Claude Belin

Institut Charles Gerhardt, UMR 5253 CNRS UM2, Agrégats,
Interfaces et Matériaux pour l'Energie, Université de
Montpellier II, Sciences et Techniques du Languedoc,
CC015, 2 Place Eugène Bataillon,
34095 Montpellier Cedex 5, France

Received October 16, 2007

Revised Manuscript Received December 20, 2007

Much effort has been devoted during the last decade to replace the graphite anode in Li-ion batteries by materials allowing more Li-storage capacity. Recently, a Li-ion battery using a tin-based electrode has reached the market.¹ Since that technological breakthrough, silicon has attracted much more attention because of an anticipated higher Li-storage specific capacity. However lithium insertion in bulk tin or silicon is associated with drastic volume change and structural modification giving rapid capacity fading. Many papers have reported research on silicon or silicon-based materials, either in amorphous or nanocrystalline forms that promise very good performance.^{2–14} In another approach, binary compounds M_xSi_{1-x} have been studied in regard to the ability of the metal to insert lithium and/or to act as a spacer to moderate lattice expansion and prevent electrode cracking.¹⁵ The chemical routes rely most frequently on mixing the pure elements with thermal annealing, ball milling, or sputtering.¹⁶

This manuscript reports a new synthesis methodology for the design of silver and silicon nanocrystalline composite electrode materials starting with a single Zintl precursor. As a first example, the preparation started with the high temperature synthesis of the Zintl compound $Li_{13}Ag_5Si_6$

followed by thermal decomposition under high vacuum to extract the whole lithium content. Thermal decomposition resulted in an optimal dispersion of silver nanocrystals inside a crystallized silicon matrix. Both $Li_{13}Ag_5Si_6$ and the nanocomposite material were evaluated as negative electrodes for Li-ion batteries. The specific capacity, 1488 mA h g^{-1} , of the composite electrode ($Ag_{0.83}Si$) was found to be twice that of $Li_{13}Ag_5Si_6$. The lithium exchange mechanism has been studied by pseudo in situ X-ray diffraction (XRD).

In our work, the intimate mixing between elements is made possible by the use of a ternary Zintl alloy as a precursor which guarantees the perfect homogeneity of the final product. The Zintl phase domain is relevant to the electrochemical processes that occur at the negative electrode during lithiation and yield binary or multinary intermetallic lithium-based phases. Their composition, structure, and stability, which were not always well understood, have been accurately determined for the Li–Zn–Ge^{17,18} and Li–Al–Si^{19,20} systems. The Li–Ag–Si system had already been investigated with five compounds reported: Li_2AgSi ,²¹ $Li_8Ag_3Si_5$,²² Li_2AgSi_2 , $Li_3Ag_2Si_3$, and $LiAg_2Si$.²³ Recently, we synthesized by the high temperature solid state route and then characterized the new compound $Li_{13}Ag_5Si_6$.²⁴ It was prepared from the elements in a tantalum weld-sealed reactor protected from oxidation at high temperature inside an evacuated silica jacket. The reactor was heated to 1000 °C, mechanically shaken to improve homogeneity, and cooled slowly to room temperature for crystallization. The resulting golden-pink alloy was examined by energy dispersive X-ray (EDX; Ag/Si = 0.82) and flame emission spectroscopy (Li/Ag = 2.62). It is a pure phase, as indicated by its XRD pattern ($R\bar{3}m$, $a = 4.391$, $c = 42.293 \text{ \AA}$). A nanocomposite material was prepared from the $Li_{13}Ag_5Si_6$ alloy as a precursor. The alloy was ground in an agate mortar to a mean particle size of 20 μm , and a weighed quantity was inserted into an alumina crucible placed in a silica reactor. Thermal treatment was carried out at 650 °C under high vacuum (10^{-6} hPa) for 24 hours to completely extract the lithium content. The loss of lithium was controlled by weighing the final product. Its composition ($Ag_{0.83}Si$) was established from atomic absorption spectrometry analysis of a weighed sample that confirmed the absence of lithium.

Soluble Zintl phases have been recently used as precursors to obtain germanium solid state mesoporous or clathrate-type networks,^{25–27} but it has long been known that silicon

- (1) Sony Corp. website (Feb. 15, 2005). <http://www.sony.net/SonyInfo/News/Press/200502/05-006E/>.
- (2) Obrovac, M. N.; Krause, L. J. *J. Electrochem. Soc.* **2007**, *154*, A103–A108.
- (3) Li, H.; Huang, X.; Chen, L.; Zhou, G.; Zhang, Z.; Yu, D.; Mo, Y. J.; Pei, N. *Solid State Ionics* **2000**, *135*, 181–191.
- (4) Graetz, J.; Ahn, C. C.; Yazami, R.; Fultz, B. *Electrochem. Solid-State Lett.* **2003**, *6*, A194–A197.
- (5) Li, J.; Dahn, J. R. *J. Electrochem. Soc.* **2007**, *154*, A156–A161.
- (6) Wang, Y. D.; Dahn, J. R. *J. Electrochem. Soc.* **2006**, *153*, A2314–A2318.
- (7) Lee, K. L.; Jung, J. Y.; Lee, S. W.; Moon, H. S.; Park, J. W. *J. Power Sources* **2004**, *129*, 270–274.
- (8) Moon, T.; Kim, C.; Park, B. *J. Power Sources* **2006**, *155*, 391–394.
- (9) Datta, M. K.; Kumta, P. N. *J. Power Sources* **2006**, *158*, 557–563.
- (10) Liu, Y.; Hanai, K.; Yang, J.; Imanishi, N.; Hirano, A.; Takeda, Y. *Electrochem. Solid-State Lett.* **2004**, *7*, A369–A372.
- (11) Zhang, Y.; Zhang, X. G.; Zhang, H. L.; Zhao, Z. G.; Li, F.; Liu, C.; Cheng, H. M. *Electrochim. Acta* **2006**, *51*, 4994–5000.
- (12) Kasavajjula, U.; Wang, C.; Appleby, A. J. *J. Power Sources* **2007**, *163*, 1003–1039.
- (13) Yang, X.; Wen, Z.; Xu, X.; Gu, Z.; Huang, S. *Electrochem. Solid-State Lett.* **2007**, *10*, A52–A55.
- (14) Yang, X.; Wen, Z.; Huang, S.; Zhu, X.; Zhang, X. *Solid State Ionics* **2006**, *177*, 2807–2810.
- (15) Dahn, J. R.; Mar, R. E.; Fleischauer, M. D.; Obrovac, M. N. *J. Electrochem. Soc.* **2006**, *153*, A1211–A1220.
- (16) Hatchard, T. D.; Obrovac, M. N.; Dahn, J. R. *J. Electrochem. Soc.* **2005**, *152*, A2335–A2344.

- (17) Sportouch, S.; Belin, C.; Tillard-Charbonnel, M.; Rovira, M. C.; Canadell, E. *New J. Chem.* **1995**, *19*, 243–251.
- (18) Lacroix-Orio, L.; Tillard, M.; Belin, C. *Solid State Sci.* **2006**, *8*, 208–215.
- (19) Spina, L.; Jia, Y. Z.; Ducourant, B.; Tillard, M.; Belin, C. Z. *Kristallogr.* **2003**, *218*, 740–746.
- (20) Tillard, M.; Belin, C.; Spina, L.; Jia, Y. Z. *Solid State Sci.* **2005**, *7*, 1125–1134.
- (21) Pauly, H.; Weiss, A.; Witte, H. Z. *Metallk.* **1968**, *59*, 47–58.
- (22) Schuster, H. U.; Seelentag, W. Z. *Naturforsch.* **1975**, *30B*, 804–804.
- (23) Kevorkov, D. G.; Pavlyuk, V.; Bodak, O. I. *Pol. J. Chem.* **1997**, *71*, 712–715.
- (24) Lacroix-Orio, L.; Tillard, M.; Belin, C. *Solid State Sci.* (doi:10.1016/j.solidstatesciences.2007.08.007).

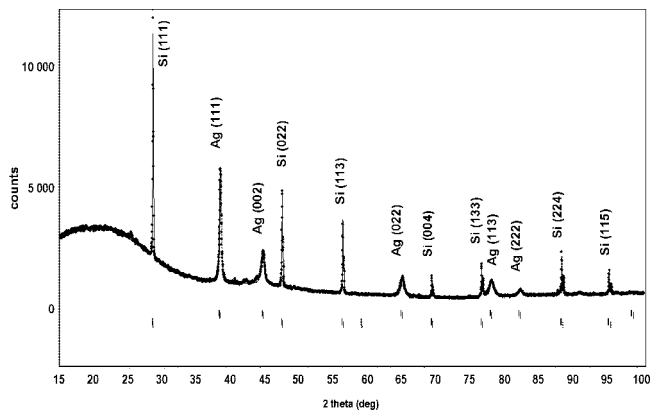


Figure 1. Experimental XRD powder pattern ($\lambda = 1.541 \text{ \AA}$) of the composite obtained from the thermal decomposition under high vacuum of the $\text{Li}_{13}\text{Ag}_5\text{Si}_6$ Zintl compound.

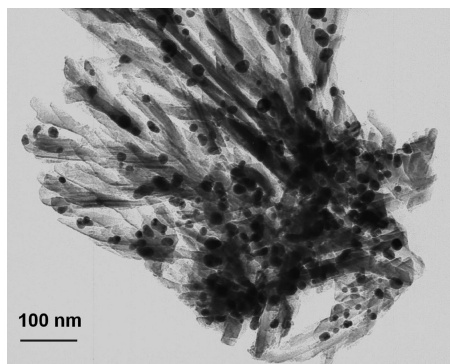


Figure 2. TEM image of the $(\text{Ag}_{0.83}\text{Si})$ composite material.

and germanium clathrate-like three-dimensional networks can be prepared by thermal decomposition of solid NaSi (NaGe) Zintl precursors.²⁸ In the present work, no clathrate-like phase could be obtained from $\text{Li}_{13}\text{Ag}_5\text{Si}_6$ which entirely decomposed into a nanostructured homogeneous dispersion of silver nanocrystals inside a crystallized silicon matrix. The morphology and the composition of the composite material were analyzed by EDX, transmission electron microscopy (TEM), and XRD.

Powder patterns were recorded on a Philips analytical X'pert diffractometer equipped with a copper tube and a hybrid monochromator (parabolic multilayer mirror and two-crystal, $\text{Cu K}\alpha_{1,2}$ radiation). TEM was carried out on a Jeol 200CX microscope operating at 120 kV. The powder was dispersed in a resin and samples prepared using a microtome, thin layers being collected on a copper grid. The diffraction pattern (Figure 1) was entirely assigned to elemental silver and silicon. In the TEM images (Figure 2), silver particles of $\sim 20 \text{ nm}$ appear dark and are very well dispersed in the silicon matrix (gray) as evidenced by EDX analysis and electron diffraction (not shown).

To compare the electrochemical performance of the $(\text{Ag}_{0.83}\text{Si})$ composite to that of the pristine $\text{Li}_{13}\text{Ag}_5\text{Si}_6$

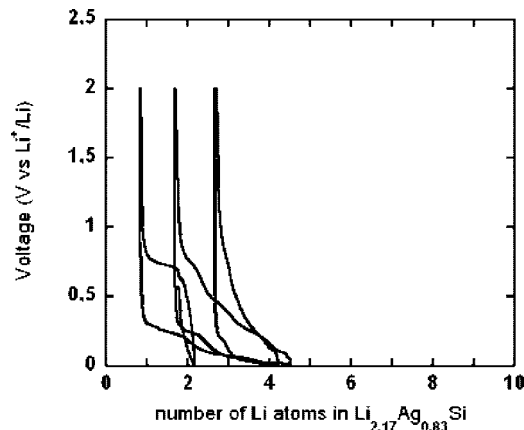


Figure 3. Voltage versus composition curves obtained in galvanostatic cycling of a $\text{Li}/\text{Li}_{13}\text{Ag}_5\text{Si}_6$ battery at a C/10 regime.

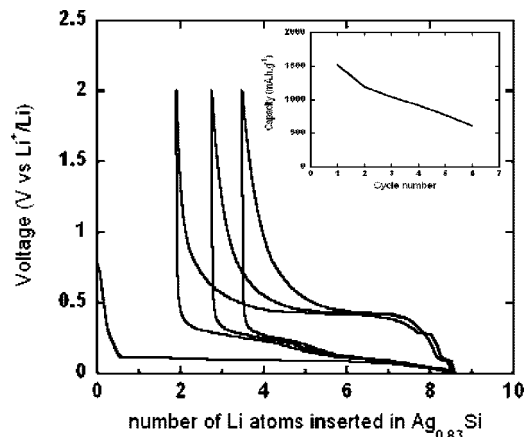


Figure 4. Voltage versus composition curves obtained in galvanostatic cycling of a $(\text{Ag}_{0.83}\text{Si})$ composite electrode at a C/10 regime.

compound, the two materials were evaluated against a pure lithium anode in electrochemical cells assembled in the inert atmosphere of an argon-filled glovebox. Electrodes comprised 85 wt % active material and 15 wt % carbon black, they were mixed intimately and pressed together without additional binder. A 1 M solution of LiPF_6 in a mixture of ethyl, propyl, and dimethyl carbonates was used as electrolyte. Charge-discharge experiments for cells Li/LiPF_6 (EC, PC, DMC)/ $\text{Li}_{13}\text{Ag}_5\text{Si}_6$, and Li/LiPF_6 (EC, PC, DMC)/ $(\text{Ag}_{0.83}\text{Si})$ were monitored with a MacPile system.

Voltage versus composition curves were obtained for the first cycles of galvanostatic experiments at the C/10 rate. As shown in Figure 3, $\text{Li}_{13}\text{Ag}_5\text{Si}_6$ ($\text{Li}_{2.17}\text{Ag}_{0.83}\text{Si}$) is able to accept additional lithium up to the formal composition $\text{Li}_{26.5}\text{Ag}_5\text{Si}_6$ ($\text{Li}_{4.40}\text{Ag}_{0.83}\text{Si}$). The limit in stoichiometry reached at the end of the subsequent charge was $\text{Li}_{5.2}\text{Ag}_5\text{Si}_6$ ($\text{Li}_{0.87}\text{Ag}_{0.83}\text{Si}$), and the reversible specific capacity was 715 mA h g^{-1} for the first cycle; however, rapid and continuous fading was observed in the following cycles.

Better results were obtained with a $\text{Ag}_{0.83}\text{Si}$ composite electrode. Starting with a discharge of the battery, lithium could be inserted to the $\text{Li}_{8.70}\text{Ag}_{0.83}\text{Si}$ limit (Figure 4). The following charge gave $\text{Li}_{2.17}\text{Ag}_{0.83}\text{Si}$. With 6.53 Li reversibly exchanged, the specific capacity of 1488 mA h g^{-1} represents a considerable improvement over the performance of the pristine ternary phase. Cycling performance of the $(\text{Ag}_{0.83}\text{Si})$

- (25) Armatas, G. S.; Kanatzidis, M. G. *Nature* **2006**, *441*, 1122–1125.
 (26) Sun, D.; Riley, A. E.; Cadby, A. J.; Richman, E. K.; Korlann, S. D.; Tolbert, S. H. *Nature* **2006**, *441*, 1126–1130.
 (27) Guloy, A. M.; Ramlau, R.; Tang, Z. J.; Schnelle, W.; Baitinger, M.; Grin, Y. *Nature* **2006**, *443*, 320–323.
 (28) Cros, C.; Pouchard, M.; Hagenmuller, P. *Bull. Soc. Chim. Fr.* **1971**, *2*, 379–386.

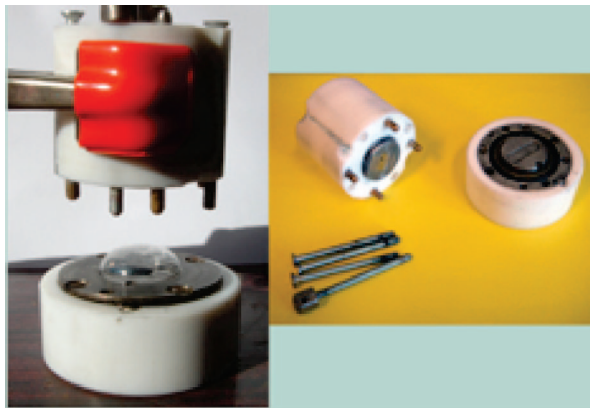


Figure 5. Electrochemical cell specially designed for pseudo in situ XRD study.

composite electrode shows that after six cycles, 50% of the initial capacity was retained which is still of the order of the specific first cycle capacity of the intermetallic electrode.

The mechanism of lithium exchange could be studied by pseudo in situ XRD using the electrochemical cell specially designed for this study. This device (Figure 5) allows separation of the active material onto its stainless support without surface damage. For the X-ray analyses, the sample was protected by a lid made from a transparent amorphous polyethylene foil. Thereafter the cell was tightly reconnected for resumption of the electrochemical cycling. During the first discharge, the electrochemical cell was opened at different steps (B, C, D) of Li insertion in the ($\text{Ag}_{0.83}\text{Si}$) electrode. At step B, the XRD pattern resembles that of the starting powder (Figure 6). It contains Si and Ag lines with a slight decrease in the Si line intensities indicating that silicon has reacted. In addition, a line ($2\theta = 25.14^\circ$) characteristic of the ternary phase $\text{Li}_x\text{Ag}_5\text{Si}_6$ begins to grow. At step C, the Ag lines have been completely replaced by those of the intermetallic compound LiAg. There is no longer any free silicon, because all has been consumed electrochemically. The intensity of the two main lines ($2\theta = 24.88$ and 41.11) of $\text{Li}_x\text{Ag}_5\text{Si}_6$ has notably increased. However, the line of low intensity at 43.6° could not be assigned to any known Li_xSi or $\text{Li}_x\text{Ag}_y\text{Si}_z$ phase nor to the compound $\text{Li}_{10}\text{Ag}_3$. At step D, the phases LiAg and $\text{Li}_x\text{Ag}_5\text{Si}_6$ are mainly present but, as indicated by the intensity decrease and the shape of the diffractogram, mostly in an amorphous form. At the end of the first charge (step E), lithium was entirely extracted from LiAg, as shown by the appearance of silver lines. It was partly extracted from the other intermetallic phases.

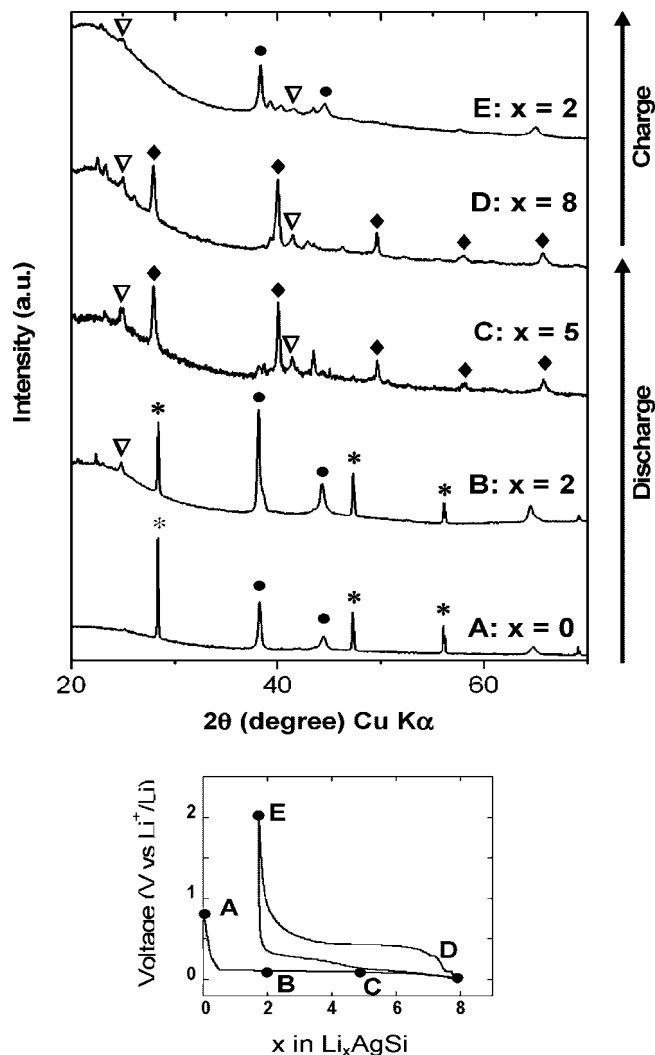


Figure 6. XRD powder patterns recorded at different steps of the galvanostatic cycle with the composite electrode (*, Si; ●, Ag; ▽, $\text{Li}_{13}\text{Ag}_5\text{Si}_6$; ◆, LiAg).

This is the first example of a new synthetic route yielding metal–silicon nanocomposites. The nanocomposite displays well-dispersed silver nanoparticles in a silicon matrix. We believe that this homogeneity is responsible for the great improvement in specific capacity. Pseudo in situ XRD showed the re-establishment of the ternary phase. This interesting mechanism is presently being studied with other systems using our methodology.

CM7029823